Brushless DC Motor: Position Linear Control Simulation

F. A. BARATA[1] J. C. QUADRADO[2] J. FERNANDO SILVA[3]
[1,2]ISEL, R. Conselheiro Emídio Navarro, 1, 1950-072 Lisboa
[3]IST, Av. Rovisco Pais 1049-001 Lisboa
CAULT, Av. Rovisco Pais 1049-001 Lisboa
PORTUGAL

Abstract: The Brushless Direct Current (BLDC) motor is one of the motors types rapidly gaining attractiveness. Actually they are becoming widely used in various consumer and industrial systems. As the name implies, BLDC motors do not use brushes for commutation, they are electronically commutated. This paper presents a Matlab simulation model that includes the control speed and position of a trapezoidal back-emf BLDC motor. The model consists of position and speed linear controllers, reference current generation, current controller and a three phase voltage inverter. Most of the applications now use a Pulse Width Modulation (PWM) current controller. The solution here proposed it new because it uses a hysteretic vectorial control in $\alpha\beta$ to control the current.

Key-Words: BLDC motor, Position control, Speed control, Current control.

1 Introduction

A brushless DC motor is a DC motor with one particularly modification, the field is on the rotor and the armature is on the stator. The brushless DC motor is actually a permanent magnet ac motor whose torque-current characteristics mimic the DC motor. Instead of commutating the armature current using brushes, electronic commutation is used [1]. This eliminates the problems associated with the brush and the commutator elements, for example, sparking and wearing out of the commutator-brush elements increasing its efficiency due to reduced losses, low maintenance and low rotor inertia, thus, making a BLDC more robust as compared to a DC motor [2].
In effect, a BLDC is a modified Permanent Magnet Synchronous Motor (PMSM) motor with the modification being that the back-emf is trapezoidal instead of being sinusoidal as in the case of PMSM[1]. These two designs eliminate the rotor copper losses, giving very high peak efficiency compared with a traditional induction motor (around 95 % and more in Nd-Fe-B machines in the 20 to 100 kW range). Besides, the power-to-weight ratio of PMSM and BLDC motor is higher than the equivalent squirrel cage induction machines. The aforementioned characteristics and a high reliability control make this type of machine a powerful traction system [3]. However, sensing the phase currents and the rotor position are the two main drawbacks of this machine.

The general type of position sensing for the BLDC motor uses to Hall-effect position sensors to detect the flux distributions of rotor magnets.
Fig. 1 illustrates the structure of a typical three-phase brushless DC motor.

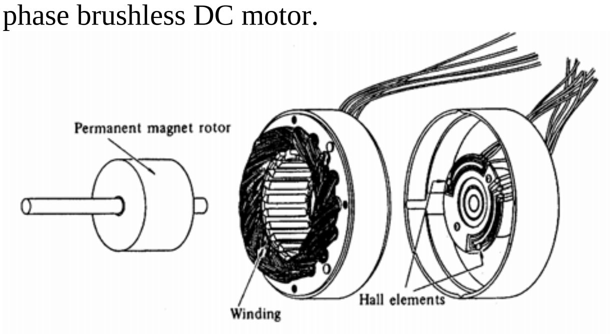

Fig. 1. Disassembled view of a brushless DC motor [4].

This paper presents a Matlab simulation model that uses linear controllers coupled to hysteretic vectorial $\alpha\beta$ current controllers, to achieve speed and position control of the BLDC motor. The basic building blocks of the system are described. The paper is organized as follows. The description of the whole system is in Section 2. The mathematical model of the BLDC motor is developed in Section 3. The operation of the hysteretic vectorial current method control is presented in Section 4. Results and conclusions are in Sections 5 and 6, respectively.

2 System descriptions

Fig. 1 shows the block diagram of the drive system under consideration.

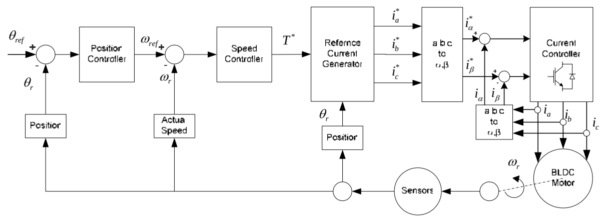

Fig. 2. System block diagram

The position of the motor, θ_r is compared with its reference value, θ_{ref}, and the position error is processed by a proportional-integral (PI) controller. This controller generates the speed reference that will be compared with the actual speed. The speed error is also processed by a PI controller.

The output of this second controller is considered the reference torque, T^*. A limit block is placed on the speed controller output. The torque will originate the value of the reference current. The reference current generator block, generates the three phase currents, i_a^*, i_b^*, i_c^* using the reference current decided by the controller and the rotor position. These currents have the shape of quasi-square wave in phase with the respective back-emf to develop constant unidirectional torque. The next block converts the three-phase reference currents in $\alpha\beta$ through the Concordia matrix. The current controller regulates the winding currents in $\alpha\beta$ within the small band around reference currents. The motor currents are compared with the reference currents and the switching commands are generated by the inverter characteristics.

3 Basic Principle of BLDC Motor

The BLDC has three stator windings and permanent magnets on the star connect rotor with no accessible neutral point. The block diagram of the BLDC motor drive is show in Fig. 3.

The analysis is based on the following assumptions [5]:

- The motor is not saturated
- Stator resistances of all windings are equal and self mutual inductances are constant.
- Power semiconductors devices in the inverter are ideal.

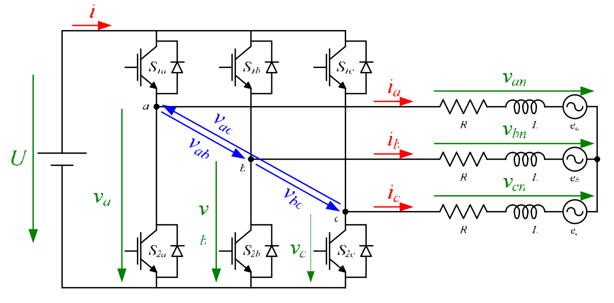

Fig. 3. Configuration of BLDC motor drive system

Under the above considerations, the circuit equations of the three windings in phase variables are given by (1).

$$\begin{bmatrix} v_a \\ v_b \\ v_c \end{bmatrix} = \begin{bmatrix} R_a & 0 & 0 \\ 0 & R_b & 0 \\ 0 & 0 & R_c \end{bmatrix} \begin{bmatrix} i_a \\ i_b \\ i_c \end{bmatrix} + \begin{bmatrix} L_a & L_{ba} & L_{ca} \\ L_{ab} & L_b & L_{cb} \\ L_{ac} & L_{bc} & L_c \end{bmatrix} \frac{d}{dt} \begin{bmatrix} i_a \\ i_b \\ i_c \end{bmatrix} + \begin{bmatrix} e_a \\ e_b \\ e_c \end{bmatrix} \quad (1)$$

In (1), R_a, R_b and R_c are the resistances of each winding, e_a, e_b and e_c are the trapezoidal shaped back-emfs and , i_a, i_b and i_c are the rectangular shaped currents as show in Fig. 4.

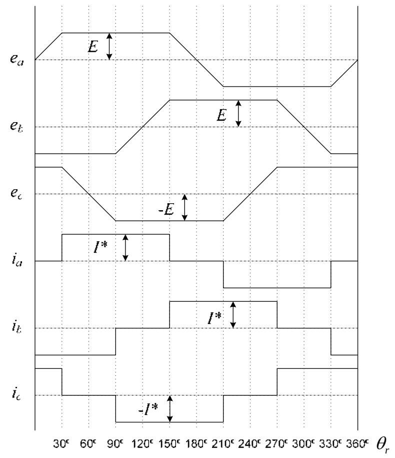

Fig. 4. Back-emf and Phase Current Waveforms.

As show in Fig. 4, the back-emfs and currents are function of rotor position (θ_r), and they have the amplitude of $E = K_e \omega_r$, (K_e is the back-emf constant) and the reference current amplitude is $I^* = T^* / K_e$. Tables 1 and 2 show how the waves are generated.

Table 1. Trabezoidal back-emf function

θ_r	e_a	e_b	e_c
0-30º	$(6E/\pi)\theta_r$	- E	E
30º-60º	E	- E	$-(6E/\pi)\theta_r+2E$
60º-90º	E	- E	$-(6E/\pi)\theta_r+2E$
90º-120º	E	$(6E/\pi)\theta_r-4E$	- E
120º-150º	E	$(6E/\pi)\theta_r-4E$	- E
150º-180º	$-(6E/\pi)\theta_r+6E$	E	- E
180º-210º	$-(6E/\pi)\theta_r+6E$	E	- E
210º-240º	- E	E	$(6E/\pi)\theta_r-8E$
240º-270º	- E	E	$(6E/\pi)\theta_r-8E$
270º-300º	- E	$-(6E/\pi)\theta_r+10E$	E
300º-330º	- E	$-(6E/\pi)\theta_r+10E$	E
330º-360º	$(6E/\pi)\theta_r+12E$	- E	E

Table 2. Reference current generation

θ_r	i_a^*	i_b^*	i_c^*
0-60º	I^*	$-I^*$	0
60º-120º	I^*	0	$-I^*$
120º-180º	0	I^*	$-I^*$
180º-240º	$-I^*$	I^*	0
240º-300º	$-I^*$	0	I^*
300º-360º	0	$-I^*$	I^*

Assuming that there is no change in the rotor reluctances with angle [6], can be considered that $L_a = L_b = L_c = L$, $R_a = R_b = R_c = R$ and $L_{ab} = L_{ba} = L_{bc} = L_{cb} = L_{ca} = L_{ac} = M$.

Considering also that, $i_a + i_b + i_c = 0$, the phase windings currents can be expressed in (2)

$$\frac{d}{dt}\begin{bmatrix} i_a \\ i_b \\ i_c \end{bmatrix} = \begin{bmatrix} 1/(L\text{-}M) & 0 & 0 \\ 0 & 1/(L\text{-}M) & 0 \\ 0 & 0 & 1/(L\text{-}M) \end{bmatrix} \cdot \left[\begin{bmatrix} v_a \\ v_b \\ v_c \end{bmatrix} - \begin{bmatrix} R & 0 & 0 \\ 0 & R & 0 \\ 0 & 0 & R \end{bmatrix}\begin{bmatrix} i_a \\ i_b \\ i_c \end{bmatrix} - \begin{bmatrix} e_a \\ e_b \\ e_c \end{bmatrix}\right] \quad (2)$$

In this kind of machine where only two of the three phases are excited through the conduction operating modes, the three-phase voltages are considered in terms of line-to-line voltages. From Fig. 5, the (3) and (4) voltage and current equations can be obtained.

$$\begin{bmatrix} v_{ab} \\ v_{bc} \\ v_{ca} \end{bmatrix} = \begin{bmatrix} R & -R & 0 \\ 0 & R & -R \\ -R & 0 & R \end{bmatrix}\begin{bmatrix} i_a \\ i_b \\ i_c \end{bmatrix} + \begin{bmatrix} (L-M) & (M-L) & 0 \\ 0 & (L-M) & (M-L) \\ (M-L) & 0 & (L-M) \end{bmatrix}\frac{d}{dt}\begin{bmatrix} i_a \\ i_b \\ i_c \end{bmatrix} + \begin{bmatrix} e_{ab} \\ e_{bc} \\ e_{ca} \end{bmatrix} \quad (3)$$

$$i_a = i_1 - i_3 \ , \ i_b = i_2 - i_1 \ , \ i_c = i_3 - i_2 \quad (4)$$

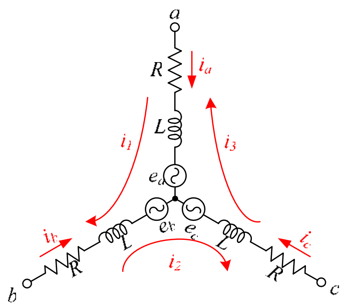

Fig. 5. Voltage and current parameters in three-phase BLDC motor

The corresponding equation for the electrical torque developed by the motor is presented in (5).

$$T_e = (e_a i_a + e_b i_b + e_c i_c)/\omega_r \quad (5)$$

The equation of motion is presented in (6)

$$\frac{d\omega_r}{dt} = (T_e - T_L - B\omega_r)/J \quad (6)$$

In (6), T_L, is the load torque, B is the viscous damping and J is the inertia.
The equations (1)-(5) were implemented in Matlab Simulink®, and the tables 1 and 2 were build with the *Lookup* table function.
The motor parameters used are show in table 3.

Table 3. Motor specifications

K_e	0.049V/(rad/sec)	L	2.72×10^{-3}H
J	0.0002kg.m^2	B	0.002 Nms
R	0.7Ω	M	-1.5×10^{-3}H
Rated Speed	1500 rpm	Poles	4

3 Current Controller Design

The Fig. 6 shows the block diagram of the implemented current controller.

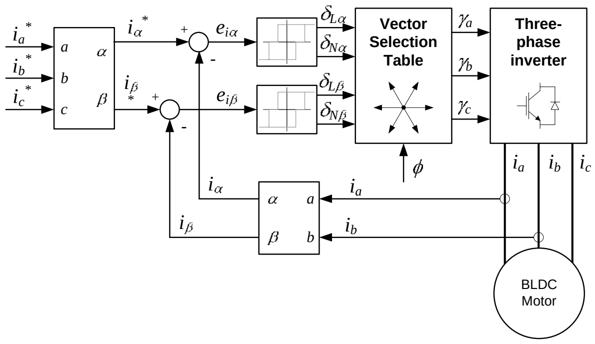

Fig. 6. Block diagram of the current controller [7]

3.1 The Three-phase Inverter

From Fig. 3, the three-phase voltages v_{an}, v_{bn} and v_{cn} is depend on the semiconductor state of each leg. The condition of the semiconductors is represented by γ_k , where $k=(a,b,c)$ and can be written as presented in (7).

$$\gamma_k = \begin{cases} 1 \rightarrow S_{1k} \text{ on and } S_{2k} \text{ off} \\ 0 \rightarrow S_{1k} \text{ off and } S_{2k} \text{ on} \end{cases} \quad (7)$$

Hence, the voltages v_a, v_b and v_c are expressed by (8).

$$v_k = \gamma_k \cdot U \qquad (8)$$

The line-to-line voltages are given by (9).

$$\begin{aligned} v_{ab} &= v_a - v_b = (\gamma_a - \gamma_b)\cdot U = v_{an} - v_{bn} \\ v_{bc} &= v_b - v_c = (\gamma_b - \gamma_c)\cdot U = v_{bn} - v_{cn} \quad (9) \\ v_{ca} &= v_c - v_a = (\gamma_c - \gamma_a)\cdot U = v_{cn} - v_{an} \end{aligned}$$

Considering (10) and operating (10) and (9), results in (11)

$$v_{an} + v_{bn} + v_{cn} = 0 \qquad (10)$$

$$v_{an} = \frac{2\gamma_a - \gamma_b - \gamma_c}{3}\cdot U \quad ; \quad v_{cn} = \frac{2\gamma_c - \gamma_a - \gamma_b}{3}\cdot U$$
$$v_{bn} = \frac{2\gamma_b - \gamma_c - \gamma_a}{3}\cdot U \qquad (11)$$

Converting to the $\alpha\beta$ referential (12) is obtained.

$$\begin{bmatrix} v_\alpha \\ v_\beta \\ v_0 \end{bmatrix} = \sqrt{\frac{2}{3}} \begin{bmatrix} 1 & -\frac{1}{2} & -\frac{1}{2} \\ 0 & \frac{\sqrt{3}}{2} & -\frac{\sqrt{3}}{2} \\ \frac{1}{\sqrt{2}} & \frac{1}{\sqrt{2}} & \frac{1}{\sqrt{2}} \end{bmatrix} \begin{bmatrix} \gamma_a \\ \gamma_b \\ \gamma_c \end{bmatrix} \quad (12)$$

Depending on the γ_k value, the voltages from the rectifier arms can assumed 2^3 possible states, that are expressed in the $\alpha\beta$ referential as

$$v_i = v_{\alpha i} + jv_{\beta i} = \begin{cases} \sqrt{\frac{2}{3}} \cdot U \cdot e^{j\frac{\pi}{3}(i-1)} (i = 1..6) \\ 0 (i = 0,7) \end{cases}$$

This expression in graphical terms is presented in Fig. (7).

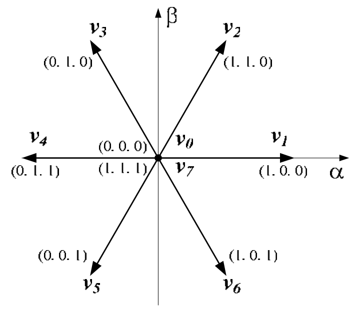

Fig. 7. The 8 possible voltages vectors in $\alpha\beta$

3.2 Current Control Strategy

Since the neutral of the machine is not accessible, the sum of the three currents in the stator is always zero $i_a + i_b + i_c = 0$. Hence, the use of two sensors is enough, being the third current obtained by $i_c = -i_a - i_b$.

The current control can be improved if $\alpha\beta$ coordinates are used. Only two hysteretic comparators are needed, because the information corresponding to the homopolar component it is not necessary. The comparators measured the error between the $\alpha\beta$ current reference and the $\alpha\beta$ current.

From Fig. 3, (13) is obtained.

$$L\frac{di_k}{dt} = v_{kn} - R\cdot i_k - e_k \qquad (13)$$

Expression (13) is in $\alpha\beta$ is represented by (14).

$$L\frac{di_{\alpha\beta}}{dt} = u_{\alpha\beta} - R \cdot i_{\alpha\beta} - e_{\alpha\beta} \qquad (14)$$

To choose one of the 8 voltage vectors (Fig. 7), it is necessary that, each hysteretic comparator evaluates the error, $e_{i\alpha\beta}$, between the $\alpha\beta$ current reference, $i_{\alpha\beta ref}$, and $\alpha\beta$ current measured, $i_{\alpha\beta}$, and quantizes the result in three discrete values [7], as presented in (15) and (16)

$$e_{i\alpha\beta} = i_{\alpha\beta ref} - i_{\alpha\beta} \qquad (15)$$

$$\begin{cases} e_{i\alpha\beta} > +\Delta \Rightarrow \delta_{\alpha\beta} = 1 \Rightarrow i_{\alpha\beta ref} > i_{\alpha\beta} \Rightarrow i_{\alpha\beta} \uparrow \Rightarrow \frac{di_{\alpha\beta}}{dt} > 0 \Rightarrow v_{\alpha\beta} > 0 \\ -\Delta < e_{i\alpha\beta} < \Delta \Rightarrow \delta_{\alpha\beta} = 0 \Rightarrow i_{\alpha\beta ref} \approx i_{\alpha\beta} \Rightarrow i_{\alpha\beta} \uparrow\downarrow \Rightarrow \frac{di_{\alpha\beta}}{dt} \approx 0 \Rightarrow v_{\alpha\beta} = 0 \\ e_{i\alpha\beta} > -\Delta \Rightarrow \delta_{\alpha\beta} = -1 \Rightarrow i_{\alpha\beta ref} < i_{\alpha\beta} \Rightarrow i_{\alpha\beta} \downarrow \Rightarrow \frac{di_{\alpha\beta}}{dt} < 0 \Rightarrow v_{\alpha\beta} < 0 \end{cases} \qquad (16)$$

In (16), Δ, represents the width of the hysteretic window , and $\delta_{\alpha\beta}$ the comparators output.

The equation (16) applied to each $e_{i\alpha\beta}$, leads to the 9 possible situations, summarized in table 4.

Table 4. Vector strategy selection

		$e_{i\alpha}$		
		$\delta_\alpha = 1$	$\delta_\alpha = 0$	$\delta_\alpha = -1$
$e_{i\beta}$	$\delta_\beta = 1$	v_2	v_2, v_3	v_3
	$\delta_\beta = 0$	v_1	v_0, v_7	v_4
	$\delta_\beta = -1$	v_6	v_5, v_6	v_5

Analysing table 4, it can be seen that there are three ambiguous situations where it is possible to apply two voltage vectors. The ambiguous situations where, $\delta_\alpha = 0$ and $\delta_\beta = 1$, $\delta_\alpha = 0$ and $\delta_\beta = -1$, can be clarified by using three level comparator, δ_β and δ_α, that can be obtained by the sum of the exit of two comparators with two different hysteretic levels, large $(\delta_{L\alpha}, \delta_{L\beta})$ and narrow $(\delta_{N\alpha}, \delta_{N\beta})$ [8]. The three level comparators are given by (17).

$$\begin{aligned} \delta_\alpha &= \delta_{L\alpha} + \delta_{N\alpha} \\ \delta_\beta &= \delta_{L\beta} + \delta_{N\beta} \end{aligned} \qquad (17)$$

The current error and the frequency of commutation of the devices are dependent on size of the hysteretic comparator window. Reduced hysteretic leads to reduce errors in the current regulation but increases the commutation frequency of the devices. The situations where $\delta_\beta = 0$ and $\delta_\alpha = 0$ can be used to minimize the number of commutations of the semiconductors [8]. This can be done applying equation (18)

$$\phi = \gamma_a \cdot \gamma_b + \gamma_b \cdot \gamma_c + \gamma_c \cdot \gamma_a \qquad (18)$$

In (18),

$$\begin{cases} \phi = 0 \Rightarrow v_0 \\ \phi = 1 \Rightarrow v_7 \end{cases}$$

Table 5 presents the voltage vector selection in function of the two and three levels comparators.

Table 5. Voltage vector selection in function of the two and three levels comparators

a	b	c	d	e	f	Vector	g	h	i
-0.5	-0.5	-0.5	-0.5	-1	-1	v_5	0	0	1
0.5	-0.5	-0.5	-0.5	0	-1	v_5	0	0	1
0.5	0.5	-0.5	-0.5	1	-1	v_6	1	0	1
-0.5	0.5	-0.5	-0.5	0	-1	v_6	1	0	1
-0.5	0.5	0.5	-0.5	0	0	$\phi = 1 \Rightarrow v_7$ $\phi = 0 \Rightarrow v_0$	1 0	1 0	1 0
0.5	0.5	0.5	-0.5	1	0	v_1	1	0	0
0.5	-0.5	0.5	-0.5	0	0	$\phi = 1 \Rightarrow v_7$ $\phi = 0 \Rightarrow v_0$	1 0	1 0	1 0
-0.5	-0.5	0.5	-0.5	-1	0	v_4	0	1	1
-0.5	-0.5	0.5	0.5	-1	1	v_3	0	1	0
0.5	-0.5	0.5	0.5	0	1	v_3	0	1	0
0.5	0.5	0.5	0.5	1	1	v_2	1	1	0
-0.5	0.5	0.5	0.5	0	1	v_2	1	1	0
-0.5	0.5	-0.5	0.5	0	0	$\phi = 1 \Rightarrow v_7$ $\phi = 0 \Rightarrow v_0$	1 0	1 0	1 0

In Table 5, a= $\delta_{L\alpha}$, b= $\delta_{N\alpha}$, c= $\delta_{L\beta}$, d= $\delta_{N\beta}$, e= δ_α , f= δ_β , g= γ_a , h= γ_b and i= γ_c .

More details about the current control strategy can be found in [7]-[8].

4 Simulation Results

To verify the proposed method, a simulation results are showed in Fig. 8. The simulation stars with a speed reference of 1500rpm, and change to -1500rpm at 0.25s. A load perturbation of 1Nm is added at 0.4s and 0.5Nm at 0.8s. The position reference of π rad occurs at 0.5s.

In Fig. 8(a), the PI controller forces the motor speed to follow the reference starting from 0.03s.

The response is smooth and there are no oscillations. It goes from 1500 to -1500rpm in 0.05s. The current waveforms, Fig 8 (b), are closed to the ones presented in Fig. 4.

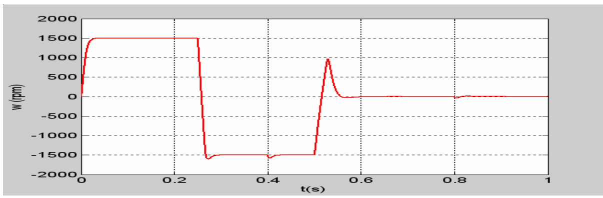

(a)

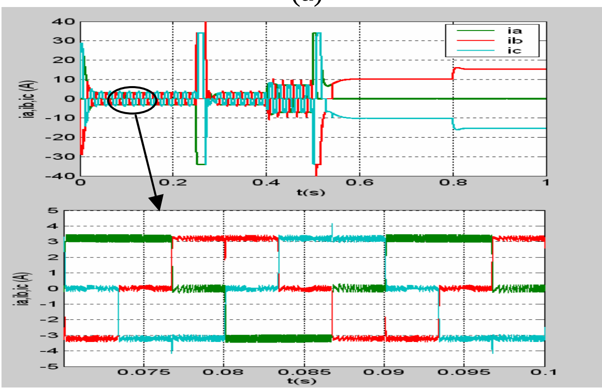

(b)

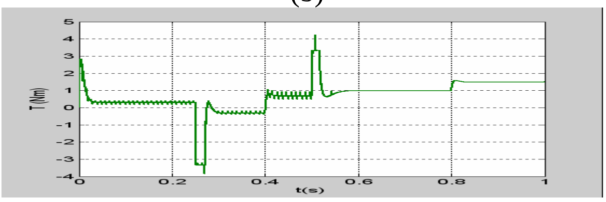

(c)

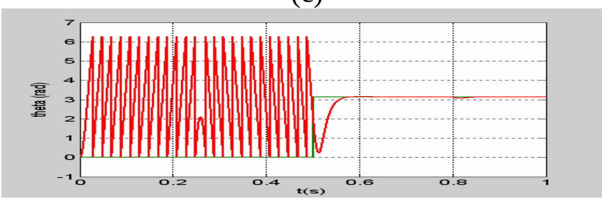

(d)

Fig 8. BLDC performance (a) Motor speed response; (b) Phase currents; (c) Torque; (d) Rotor position(θ_r);

The noise observed in the current and torque waveforms, Fig. 8(b) and (c), is due to the commutation points created by the current reference when changes from 0 to I^* and from 0 to $-I^*$ instantaneous. After the position step at 0.5s the speed decreases and changes from -1500rpm to 0 in 0.1s Fig. 8(a). As expected, in Fig 8(b) and Fig. 8(c) the current and torque remain constants as soon as the rotor attains the reference position, at 0.6s, can be notice that in both situations, the ripple is small enough. The load perturbations are almost not visible in the speed and position, but can be seen in the torque and current by their increase.

5 Conclusions

The performance of a BLDC motor driven by a hysteretic vectorial controller in αβ, is considered in alternative to the PWM inverter [3,6,9] , offering an efficient and faster alternative approach in the design of such drive system . The corresponding current, torque, position and speed performances using the proposed control method were simulated and validated. The proposed controller design, allows a straight forward application of these machines.

Future work includes experimental validation of this approach and comparison with another drive systems models and control techniques.

References:

[1] Khopkar, R.V., "DC-DC Converter Current source Fed Naturally Commutated Brushless DC Motor Drive", Master of Science Thesis, Texas A&M University, College Station, TX, August 2003.

[2] Shing, B., Singh, B., Jain, K., "Implementation of DSP based Digital Speed Controller for Permanent Magnet Brushless DC Motor" *IE(I) Journal-EL*, Vol. 84, Jun. 2003, pp 16-21.

[3] Dixon J.W., Rodríguez, M., Huerta, R., "Simplified Sensorless Control for BLDC Motor", *The 19th International Battery, Hybrid and Fuel Cell Electric Vehicle Symposium* , October 2002, Bexco, Busan, Korea.

[4] Zhu, J.G., *Chapter 12. Brushless Motors*, Electromechanical Systems, University of Technology, Sydney Faculty of Engineering.

[5] Park, S-I, Kim, T-S, Ahn, S-C, Hyun D-S. "An Improved Current Control Method for Torque Improvement of High Speed BLDC Motor" *Proc. of IEEE APEC2003*, Vol. 1, , Feb. 2003, pp. 294-299.

[6] Pillay, P., Krishnan, R., "Modelling, Simulation and Analysis of a Permanent Magnet Brushless DC Motor Drive." *Conference Record of IEEE/IAS Meeting*, 1987, p 8.

[7] Luís R., *Posicionador Electromecânico Linear*, Controlo de Conversores Comutados, IST, Lisboa, 2005 (in Portuguese).

[8] Silva, J.F., *Inversores trifásicos de tensão*, Controlo de Conversores Comutados, IST, Lisboa, 2004 (in Portuguese).

[9] Lee, C. K., Luk, P. C. K., "Efficient Modelling for a DC Motor Driver" *Proc. of IEEE* 1994, pp. 188-191.